Synthesis, Structure, Spectroscopic Studies, and Complexation of Novel Crown Ether Butadienyl Dyes

by **Sergey P. Gromov***[a]), **Artem I. Vedernikov**[a]), **Evgeny N. Ushakov**[b]), **Lyudmila G. Kuz'mina**[c]), **Alexei V. Feofanov**[d]), **Vitaly G. Avakyan**[a]), **Andrei V. Churakov**[c]), **Yurii S. Alaverdyan**[d]), **Ekaterina V. Malysheva**[b]), **Michael V. Alfimov**[a]), **Judith A. K. Howard**[e]), **Bertil Eliasson**[f]), and **Ulf G. Edlund***[f])

[a]) Photochemistry Center, Russian Academy of Sciences, 7A Novatorovstr., Moscow 117421, Russia (fax: (095) 936 1255; e-mail: gromov@photonics.ru)

[b]) Institute of Problems of Chemical Physics, Russian Academy of Sciences, Chernogolovka 142432, Moscow Region, Russia

[c]) N. S. Kurnakov Institute of General and Inorganic Chemistry, Russian Academy of Sciences, 31 Leninsky prosp., Moscow 117907, Russia

[d]) Shemyakin-Ovchinnikov Institute of Bioorganic Chemistry, Russian Academy of Sciences, 16/10 Miklukho-Maklayastr., Moscow 117997, Russia

[e]) Chemistry Department, Durham University, South Road, Durham DH1 3LE, UK

[f]) Department of Organic Chemistry, Umeå University, SE-901 87, Umeå, Sweden (fax: +46-90-7867844; e-mail: Ulf.Edlund@chem.umu.se)

Dedicated to Professor *André M. Braun* on the occasion of his 60th birthday

Butadienyl dyes of the benzothiazole series with various fragments of benzocrown ethers **1a**–**c** were synthesized for the first time. The structures and spectral properties of crown-containing butadienyl dyes and their complexes with alkali and alkaline-earth metal cations were studied by X-ray diffraction analysis and ^{1}H-NMR, UV/VIS, and resonance *Raman* spectroscopy. To interpret the experimental results, quantum-chemical calculations were performed. In the case of Sr^{2+} and Ba^{2+} ions, the formation of strong sandwich complexes $[M(\mathbf{1b})_2]^{2+}$ of an unusual structure involving stacking interactions was established; the dye molecules are arranged one above another in the complex according to the 'head-to-head' pattern.

1. Introduction. – Crown compounds containing a chromophore conjugated with the macrocycle serve as selective photosensitive complexones for metal cations [1][2]. It was shown previously that crown-containing styryl dyes (CSD), in particular dye **I** [3], bind metal ions and that complex formation changes the spectral and photochemical characteristics of the dyes. Dyes of this type have been used for the development of novel photochemical and photophysical molecular devices [4–7]. An increase in the length of the chain of conjugation in polymethine dyes from $n = 1$ to $n = 2$ is known to induce a 20–30 nm bathochromic shift of the long-wavelength absorption maximum and to increase noticeably the fluorescence quantum yield [8]. Indeed, butadienyl dyes exhibit fairly efficient fluorescence and are able to generate laser radiation on pulse excitation [9][10]. It can be suggested that a combination of the structural fragment of a butadienyl dye and a macroheterocyclic fragment would provide a new promising type of light-sensitive host molecule, which can be used as selective chromo- and fluoroionophores, as elements of photoswitchable molecular devices, and for improving the generation characteristics of laser dyes. However, crown-containing butadienyl dyes (CBD) have not been described in the literature.

Recently [11], we reported the synthesis of the first representatives of CBD, in particular of dye **II**, in which the positively charged heterocyclic residue and a phenylazacrown fragment are linked *via* a butadiene spacer. Despite the relatively low cation-binding ability of these dyes, they have demonstrated a series of promising properties as regards practical application [12].

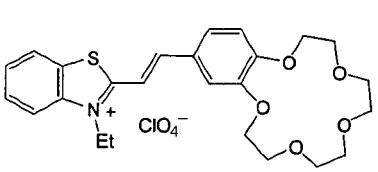

I (*E*)

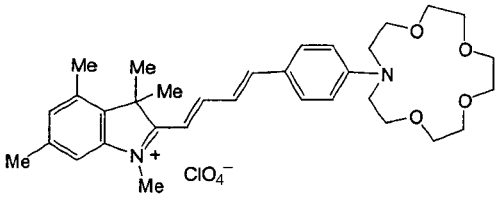

II (*E,E*)

On passing from phenylazacrown-containing to benzocrown-containing CSD, the stability constants for complexation with alkaline-earth metal cations are known to increase by approximately two orders of magnitude [13]. It appeared of interest to develop a synthesis and to study the structural, spectral, and complex-forming properties of a new series of butadienyl dyes containing a benzocrown fragment.

2. Results and Discussion. – 2.1. *Synthesis and Structure of Dyes.* 2.1.1. *Synthesis.* We prepared dyes **1a**–**c** containing benzo[12(or 15 or 18)]crown-4(or 5 or 6) fragments and dye **1d** containing two MeO groups, the latter two representing the electron-donating effect of a crown-ether fragment. Unlike CBDs **1a**–**c**, compound **1d** is not expected to be prone to form complexes with metal cations. To synthesize dyes **1a**–**d**, we developed a two-step synthesis of crown-containing cinnamaldehydes **3a**–**d** from the corresponding crown-containing benzaldehydes and dimethoxybenzaldehyde [14]. Butadienyl dyes **1a**–**c** were prepared in 30–39% yields by condensation of the crown-containing cinnamaldehydes **3a**–**c** with the quaternary benzothiazolium salt **2** [11] on prolonged refluxing in anhydrous EtOH (*Scheme 1*).

Butadienyl dye **1d** was prepared in a similar way from dimethoxycinnamaldehyde **3d** and benzothiazolium salt **2** (*Scheme 2*).

The use of pyridine or Ac_2O as a catalyst in this synthesis [11] resulted in the formation of a styryl-dye impurity, for example **I** (according to ^{1}H-NMR), which was difficult to separate; apparently, this is due to the transformation of cinnamaldehydes **3** into the corresponding benzaldehydes, which then react with **2** to give rise to styryl dyes.

2.1.2. *NMR Data*. The structures of compounds **1a**–**d** were established by ^{1}H-NMR spectroscopy. The data of elemental analysis correspond to the proposed structures. The ^{1}H-NMR signals of the compounds were assigned by means of NOESY data and the data of homonuclear correlation spectroscopy between ^{1}H nuclei. According to spin-spin coupling constants, dyes **1a**–**d** in (D_6)DMSO have the (*E*,*E*) configuration (^3J(H–C(a),H–C(b)) = 14.7–14.8 Hz, ^3J(H–C(c),H–C(d)) = 15.3–15.6 Hz) and the *s-trans* conformation (^3J(H–C(b),H–C(c)) = 10.4–10.5 Hz), which are similar to those established by corresponding coupling constants in dye **II** [11]. The NOESY data for dye **1b** in CD_3CN suggest that this dye exists in this solvent mainly in the *syn*-

Scheme 1

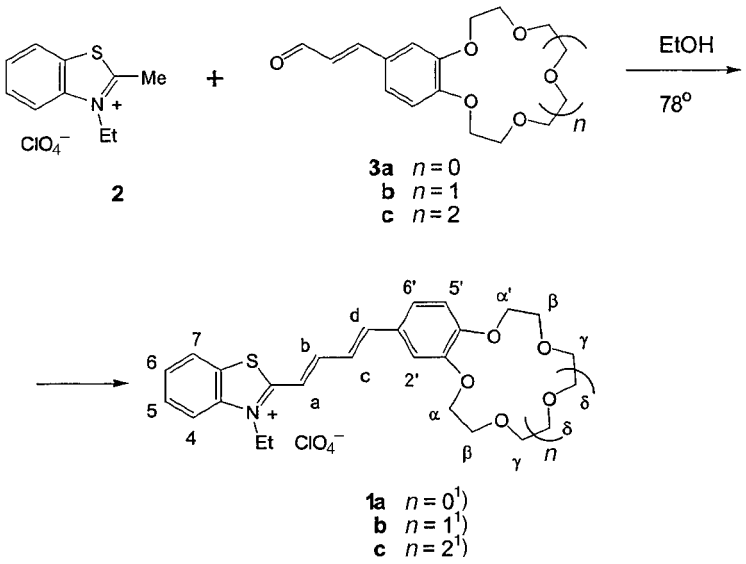

2

3a $n = 0$
b $n = 1$
c $n = 2$

1a $n = 0$[1])
b $n = 1$[1])
c $n = 2$[1])

Scheme 2

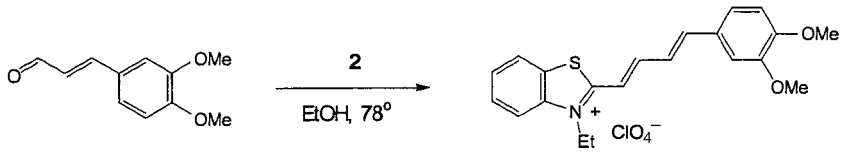

3d **1d**

(*E*,*E*)-**1b** conformation, although this cannot be claimed with confidence due to some overlap of the H–C(2′) and H–C(6′) ^{1}H-NMR signals. According to NOESY data for **1b** in $CDCl_3$, this dye exists as an equilibrium mixture of two conformers, *syn*-(*E*,*E*)- and *anti*-(*E*,*E*)-**1b** (see *Scheme 3*), which is in line with the data obtained previously for CSD **I** [15].

2.1.3. *Modeling*. The conformational equilibrium between the *syn*-(*E*,*E*)- and *anti*-(*E*,*E*)-**1b** was calculated by PM3, DFT, and ZINDO/S quantum-chemical methods (see *Exper. Part*). The butadiene part of the dye molecule has five rotational degrees of freedom, which corresponds to 32 rotational isomers differing one from another in their dihedral angles. Each of the 32 structures was fully optimized by the PM3 method and characterized by a set of $3N-6$ ($N=66$ atoms) positive harmonic vibrational frequencies, indicating that each structure corresponds to a local minimum on the potential-energy surface (PES). Two of the structures correspond to a global minimum, namely completely *transoid anti*- and *syn*-forms of **1b** (*Scheme 3*), the energy difference between them being only 0.16 kcal/mol in favor of the *syn*-form. This means that, at room temperature, the two forms should occur in equilibrium. All the

[1]) Arbitrary numbering; for systematic names, see *Exper. Part.*

Scheme 3

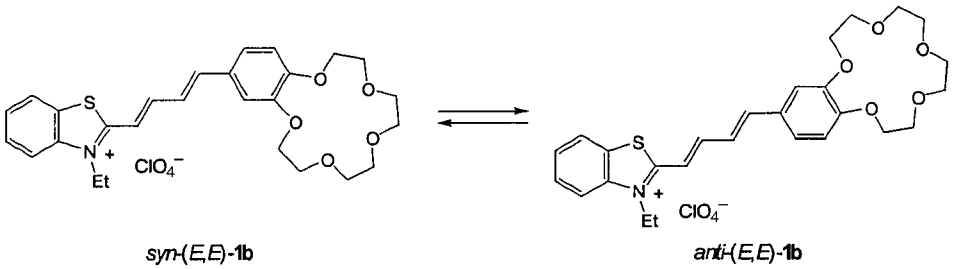

dihedral angles in the unsaturated fragments of these two isomers occur in the range of 0–2°. A DFT calculation for the *anti*-(*E*,*E*)- and *syn*-(*E*,*E*)-**1b** performed with full geometry optimization showed that the energies of these isomers are also close (*Table 1*). The results of calculations of the bond lengths and dihedral angles in *syn*-(*E*,*E*)-**1b** are in good agreement with the X-ray diffraction data for *syn*-(*E*,*E*)-**1c** that we obtained.

Table 1. *Total Energies (*E_{total}*) Zero-Point Vibration Energies in the Harmonic Approximation (ZPE) Energies at 0 K (*E_0*)*[a]*) and* ΔE[b]*) for* **1b** *and Its* Mg^{2+} *Complexes Calculated by the DFT Method*

	E_{total}/hartree	*ZPE*/hartree	E_0/hartree[a])	ΔE (*anti*- and *syn*-isomers) kcal/mol[b])
anti-(*E*,*E*)-**1b**	– 1875.514864	0.532380	– 1874.982484	0.3
syn-(*E*,*E*)-**1b**	– 1875.515615	0.532575	– 1874.983041	0.0
[Mg{*anti*-(*E*,*E*)-**1b**}]$^{2+}$	– 2074.949012	0.537234	– 2074.411778	– 2.0
[Mg{*syn*-(*E*,*E*)-**1b**}]$^{2+}$	– 2074.945853	0.537225	– 2074.408627	0.0

[a]) $E_0 = E_{total} + ZPE$; [b]) The relative energy of the *anti*- and *syn*-isomers, $\Delta E = E_{0anti} - E_{0syn}$.

2.1.4. *X-Ray Crystallography.* We succeeded in growing the single crystals of dye **1c**. The independent part of the crystal unit cell of **1c** includes a positively charged dye molecule, a perchlorate anion, an MeCN solvent molecule, and a H_2O molecule. The H_2O molecule is coordinated to the crown ether *via* two H-bonds, one of which is bifurcated. The perchlorate anions and MeCN solvent molecules occupy cavities in the dye molecular packing. Two views of the structure of the dye molecule, together with the coordinated H_2O molecule are shown in *Fig. 1*.

The molecule is nearly planar. Three strictly planar subunits can be distinguished, namely, the benzothiazolium system (plane *1*), the butadiene system (plane *2*), and the benzene ring of the benzocrown ether system (plane *3*). The dihedral angles between the planes *1* and *2* and *2* and *3* are 5.0 and 6.2°, respectively. This geometry is favorable for extensive conjugation of π-electrons over the two aromatic and butadiene systems of the molecule. In the butadiene subunit, two formally double bonds, C(17)–C(18) and C(19)–C(20), are longer (1.349(4) and 1.357(4) Å) and one formally single bond, C(18)–C(19), is shorter (1.427(5) Å) than the bonds commonly observed for C=C–C(Ar) fragments (1.339 Å and 1.455 Å, resp.), indicating conjugation in the butadiene fragment [16][17]. The two other formally single bonds, C(14)–C(17)

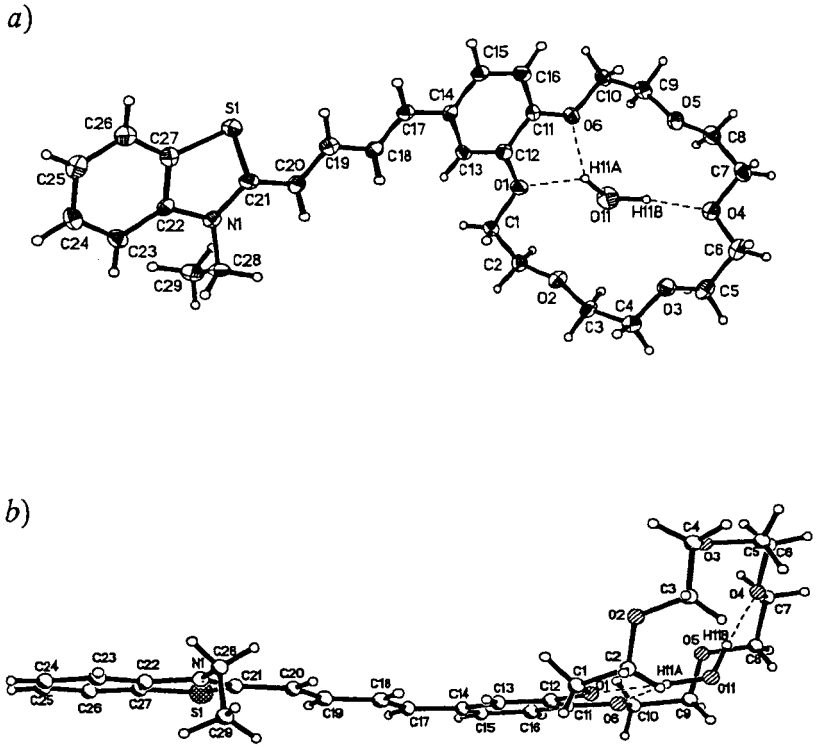

Fig. 1. *Structure of the water complex of* **1c** *showing 50% probability of thermal anisotropic atom displacement parameters:* a) *the frontal and* b) *the side projections.* Arbitrary numbering.

(1.457 Å) and C(20)–C(21) (1.437(4) Å), are *ca.* 1.455 Å long. The conjugation in the butadiene subunit of **1c** is less pronounced than that in previously investigated butadienyl dye **II**. In **II**, the bond lengths in the butadiene fragment range within 1.358–1.380 and 1.418–1.419 Å, for two independent molecules. However, two formally single C–C bonds between butadiene and both substituent subunits (1.450(6)–1.445(6) and 1.409(6)–1.401(6) Å, resp.) are close to those found for **1c**.

The benzene ring in the benzocrown system of **1c** exhibits bond-length redistribution. Evident bond-length alternation is observed in the C(11)–C(12)–C(13)–C(14) fragment (1.414(4), 1.377(4), and 1.416(4) Å, resp.). Meanwhile, almost complete bond-length delocalization is found in the other half of this benzene ring, C(11)–C(16)–C(15)–C(14) (1.382(4), 1.393(4), and 1.389(4) Å, resp.). This bond-length distribution indicates a contribution of the resonance structure shown in the *Formula syn-*(*E*,*E*)-**1c**.

Conversely, the benzene ring of the phenylazacrown system of **II** displays a pronounced *para*-quinoid pattern. This distribution of bond lengths appears to result from the involvement of the lone electron pair at the N-atom in the conjugation with the benzene ring (see *Formula* **II**). Apparently, the difference between the geometries of *syn*-(*E*,*E*)-**1c** and **II** is caused by different electronic effects of the crown-ether substituents (benzocrown and phenylazacrown, resp.). In **II**, the lone electron pair at

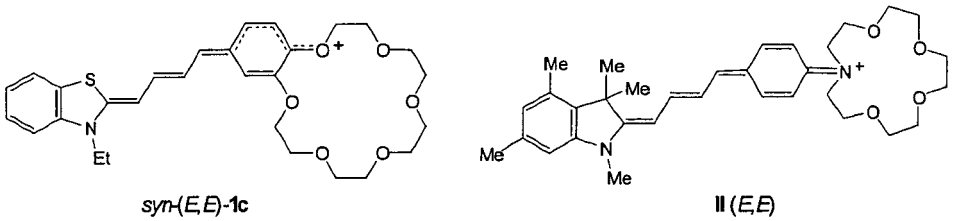

syn-(*E*,*E*)-**1c** II (*E*,*E*)

the N-atom is involved in the conjugation with the benzene ring, whereas in **1c**, both O-atoms, O(1) and O(6), have a geometry favorable for their conjugation with the π-system of the benzene ring. Actually, the bond angles at the O(1) and O(6) atoms (117.5(2) and 116.4(2)°, resp.) imply the sp^2 hybridization state of these atoms, unlike the bond angles at O(2), O(3), O(4), and O(5) (113.0(2), 111.6(2), 112.1(3), and 112.3(2)°, resp.), which are typical of the sp^3 hybridization state of these O-atoms. With this hybridization state of O(1) and O(6), the C(1)–O(1)–C(12)–C(13) and C(10)–O(6)–C(11)–C(16) torsion angles (–2.6 and 3.4°, resp.) are close to the values most suitable for the conjugation of the p orbitals (p is the orbital of a lone pair) of the O(1) and O(6) atoms with the benzene ring π-system. However, these particular O-atoms are simultaneously involved in a H-bond with the H_2O molecule. The same H-atom H(11A) of the H_2O molecule forms a bifurcate H-bond with both O(1) and O(6) atoms. The corresponding distances are equal to 2.11(7) and 2.09(7) Å, respectively. The second H-atom of the H_2O molecule, H(11B), participates in another H-bond with the O(4) atom (H···O 1.86(7) Å). Thus, the real bond-length distribution in the benzene ring of **1c** is a consequence of a compromise between two opposite effects, namely, the conjugation of the lone electron pairs at O(1) and O(6) with the benzene ring and the participation of these lone pairs in the H-bonds with the H_2O molecule. The O-atoms of the [18]crown-6 subunit form an almost regular hexagon, with the short diagonals varying within 2.594–2.964 Å. The mean plane of the O-atoms is inclined with respect to the benzene ring plane by 43.7° (*Fig. 1,b*). The O(11) atom of H_2O is displaced from the mean plane of the crown-ether O-atoms by 1.61 Å.

In the benzothiazolium fragment, the N(1)–C(21) bond (1.344(4) Å) is shorter than the N(1)–C(22) bond (1.400(4) Å), which is indicative of essential localization of the double bond. However, all bond lengths in the benzothiazolium fragment fall within typical values [16].

In the crystal of **1c**, the conjugated molecules form centrosymmetrically related couples due to stacking interactions in which the molecules are arranged according to the 'head-to-tail' pattern. The interplanar spacing between the mean planes of the molecules in a couple is equal to 3.69 Å. These couples are arranged in 'staircases' (*Fig. 2,a*).

The axes of adjacent 'staircases' are almost perpendicular to one another, as shown in *Fig. 2,b*, in which double lines denote the couple of molecules and arrows show the 'staircase' direction.

This mutual arrangement of the molecules corresponds to both the herringbone and stacking geometries, which are equally typical of the crystal packing of large aromatic molecules [17]. Such packing is exemplified by pyrene and perylene and referred to as a

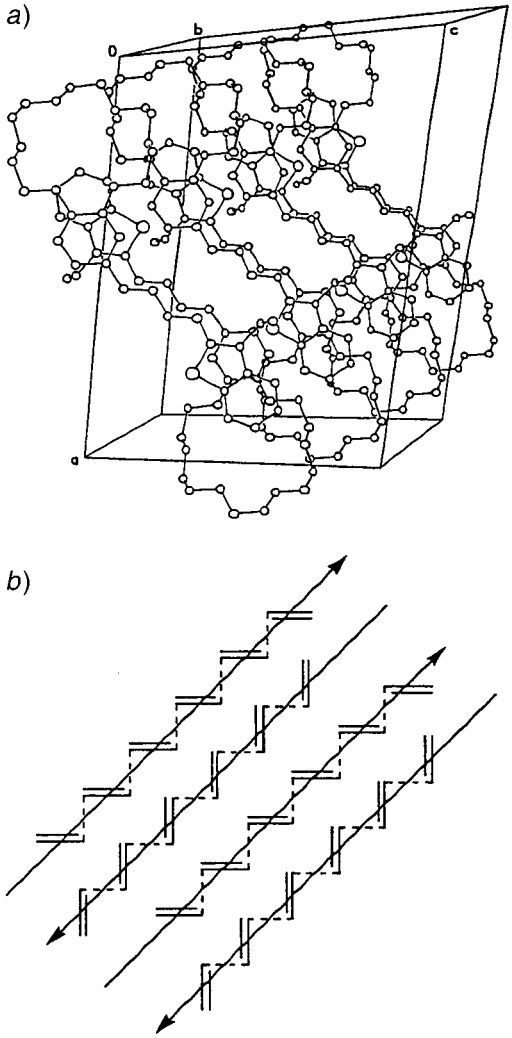

Fig. 2. a) *Stacking pairs of molecules* **1c** *belonging to a 'staircase' with respect to the crystal unit cell.* b) *Antiparallel axes of adjacent 'staircases'.*

'sandwich-herringbone' packing. Previously, this type of packing has not been observed for either crown-ether styryl or butadienyl dye molecules. However, channels of loose packing formed by the crown-ether subunits, characteristic of all the crystal structures of crown-ether dyes investigated previously, are also found in this structure.

2.2. *Spectroscopic Characterizations.* 2.2.1. *Neutral Molecules. Table 2* presents the electronic spectroscopy data for dyes **1a**–**d** and for the previously studied styryl dye **I**. The butadienyl dyes **1a**–**d** exhibit similar spectroscopic properties. A distinctive feature of the absorption spectrum of **1a** is a hypsochromic shift and the relatively low intensity of the long-wavelength band, which is apparently due to some disturbance of

the conjugation of two O-atoms of the [12]crown-4 fragment, caused by the small size of the macrocycle, with the rest of the chromophore system. Comparison of the data for **1b** and **I** shows that extension of the polymethine chain in the dye results in an increase in the intensity of the long-wavelength absorption band, a substantial bathochromic shift of the absorption and luminescence maxima, and an increase in the *Stokes* shift from 5140 to 6010 cm^{-1}. The luminescence quantum yield also increases; however, nonradiative deactivation of the electronically excited state still predominates. In the case of CSD, the major channel of nonradiative deactivation is *trans-cis* isomerization [2]. Most likely, the relatively low luminescence quantum yield for **1b** is also due to this reaction. The results of studies of photoisomerization of **1a**–**c** will be published elsewhere.

2.2.2. *Complexes.* The addition of alkali and alkaline earth metal perchlorates to an MeCN solution of **1a**–**c** induced a substantial ($\Delta\lambda$ up to 39 nm) hypsochromic shift of the long-wavelength absorption maximum (*Fig. 3*), which can be attributed to charge redistribution in the chromophore part of the dye caused by the interaction of the crown-ether fragment with the metal cation.

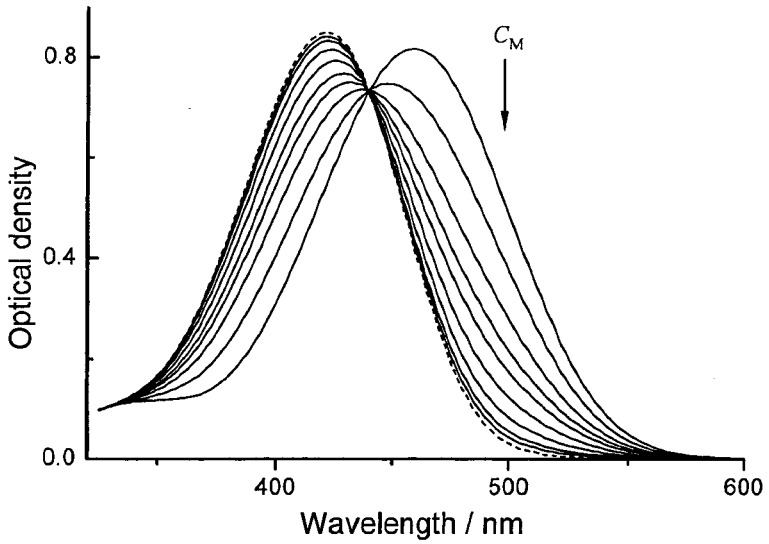

Fig. 3. *Absorption spectra of* **1b** *in MeCN* ($3.1 \cdot 10^{-6}$ M, 5.5-cm cell) *measured at various concentrations of* Mg^{2+} *ranging from 0 to* $5 \cdot 10^{-5}$ M. The ionic strength of the solution was maintained constant (0.01M) with Et_4NClO_4. The dashed curve is the spectrum of complex $[Mg(\mathbf{1b})]^{2+}$.

In the case of dye **1d**, the shift of the long-wavelength absorption maximum did not exceed 1 nm even for high concentrations of metal salts (*ca.* 0.1M), indicating that **1d** does not react with metal cations.

To determine the number of absorbing components in the metal/dye systems, the data matrices composed of the absorption spectra, measured at a constant dye concentration and different metal-cation concentrations, were subjected to the singular-value-decomposition (SVD) procedure [19]. For the majority of systems, the experimental matrices were reconstructed with high accuracy ($\sigma D < 0.001$) by means

of two significant SVD vectors, which implied the presence of only two absorbing components in these systems. In the case of **1b** with Ba^{2+} or Sr^{2+}, the SVD analysis indicated the presence of a third absorbing component, the contribution of which increased with an increase in the dye concentration. *Fig. 4* shows the absorption spectra of **1b** measured at $C_L = 7 \cdot 10^{-5}$ M and various Ba^{2+} concentrations; the absence of an isosbestic point in these spectra indicates that the system contains more than two absorbing components.

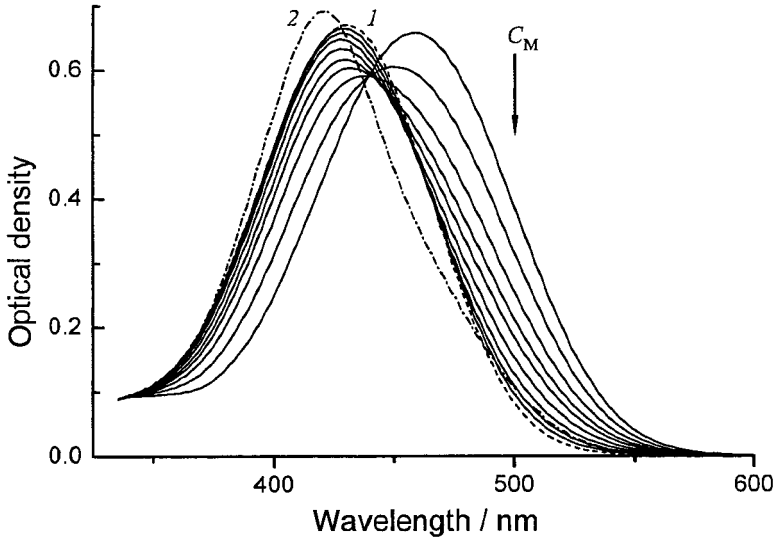

Fig. 4. *Absorption spectra of dye* **1b** *in MeCN* ($C_L = 7.0 \cdot 10^{-5}$ M, 0.2-cm cell) *measured at various concentrations of* Ba^{2+} *ranging from 0 to* $6.3 \cdot 10^{-4}$ M. The ionic strength of the solution was maintained at 0.01M with Et_4NClO_4. Curves *1* and *2* are the calculated spectra of complexes $[Ba(\mathbf{1b})]^{2+}$ and $[Ba(\mathbf{1b})_2]^{2+}$, respectively.

It is known that [15]crown-5 ethers are prone to form sandwich (2:1) complexes with large metal cations [5][20]. It is quite probable that the presence of a third absorbing component in the case of **1b** with Sr^{2+} and Ba^{2+} is due to the presence of complexes of this type.

To verify this assumption, the spectroscopic-data matrices obtained for **1b** with Sr^{2+} or Ba^{2+} were reconstructed from the complexation model involving the two equilibria of *Eqns. 1* and *2* where L is the dye, M is the metal cation, and K_1 and K_2 are the complex stability constants. The reconstruction was performed by the matrix self-modeling method [6], which allows the complex stability constants and the unknown spectra of absorbing components to be calculated simultaneously.

$$L + M \overset{K_1}{\rightleftharpoons} LM \tag{1}$$

$$LM + L \overset{K_2}{\rightleftharpoons} L_2M \tag{2}$$

For both Sr^{2+} and for Ba^{2+}, the data matrix composed of three sets of spectra measured at $C_L = 3 \cdot 10^{-6}$, $1.5 \cdot 10^{-5}$, and $7 \cdot 10^{-5}$ M in quartz cells of different lengths was reconstructed within a very small total residual error ($\delta_D < 0.002$, optical-density units), indicating that the above reaction model holds. For the other metal/dye systems studied, the spectroscopic-data matrices were reconstructed well from a 1:1 complexation model (*Eqn. 1*). The spectroscopic parameters and the stability constants for the metal complexes of **1a**–**c** are listed in *Tables 2* and *3*, respectively. *Table 2* presents also the results of direct measurements of the luminescence characteristics of 1:1 complexes of **1b** with alkaline earth metal cations. These measurements were performed at $C_L = 5 \cdot 10^{-6}$ M and $C_M = 5 \cdot 10^{-3}$ M (under these conditions, the equilibrium is completely shifted toward 1:1 complexes, even for large metal cations). Comparison of the data for **1b** and **II** shows that, owing to the use of a benzocrown fragment in place of the *N*-phenylazacrown one in the butadienyl dye, the stability constants of metal complexes increase by more than two orders of magnitude. In the case of **1b**, complexation induces a smaller shift of the absorption band but a markedly greater blue shift of the luminescence band.

Table 2. *Absorption and Luminescence Spectroscopy Data for Dyes* **I**, **II**, **1a**–**d**, *and Their Metal Complexes*[a])

	Absorption			Luminescence		
	λ_{max}/nm	$\Delta\lambda_{max}$[b])/nm (cm^{-1})	$\varepsilon_{max} \cdot 10^{-4}/M^{-1}\,cm^{-1}$	λ_{max}/nm	$\Delta\lambda_{max}$[b])/nm (cm^{-1})	$\varphi_f \cdot 10^3$[c])
I	430		4.07	552		6.3
[Mg(**I**)]$^{2+}$	392	– 38 (2250)	3.88	498	– 54 (1960)	2.2
[Ca(**I**)]$^{2+}$	393	– 37 (2190)	3.88			
[Sr(**I**)]$^{2+}$	397	– 33 (1930)	3.90			
[Ba(**I**)]$^{2+}$	402	– 28 (1620)	3.93	519	– 33 (1150)	3.1
II	585		6.73	703		50
[Li(**II**)]$^{+}$	543	– 42	5.45	694	– 7	98
[Na(**II**)]$^{+}$	519	– 66	4.71	699	– 4	91
[Ca(**II**)]$^{2+}$	450	– 135	4.74	691	– 12	80
1a	447		3.66			
[Li(**1a**)]$^{+}$	424	– 23	3.75			
[Na(**1a**)]$^{+}$	431	– 16	3.73			
1b	459		4.73	634		14
[Li(**1b**)]$^{+}$	441	– 18	4.85			
[Na(**1b**)]$^{+}$	440	– 19	4.86			
[K(**1b**)]$^{+}$	447	– 12	4.79			
[Mg(**1b**)]$^{2+}$	421	– 38 (1970)	4.92	567	– 67 (1860)	1.6
[Ca(**1b**)]$^{2+}$	422	– 37 (1910)	4.91	580	– 54 (1470)	2.0
[Sr(**1b**)]$^{2+}$	426	– 33 (1690)	4.82	587	– 47 (1260)	2.6
[Ba(**1b**)]$^{2+}$	430	– 29 (1470)	4.82	598	– 36 (950)	3.2
[Sr(**1b**)$_2$]$^{2+}$	420	– 39 (2020)	9.87			
[Ba(**1b**)$_2$]$^{2+}$	421	– 38 (1960)	9.94			
1c	463		4.86			
[Li(**1c**)]$^{+}$	451	– 12	4.86			
[Na(**1c**)]$^{+}$	452	– 11	4.89			
[K(**1c**)]$^{+}$	449	– 14	4.91			
1d	459		4.91			

[a]) In MeCN; the data for dye **I**, except for the luminescence parameters of [Mg(**I**)]$^{2+}$, are taken from [18]; the data for dye **II** are taken from [11]. [b]) Shift of the spectral maximum upon complexation. [c]) Luminescence quantum yield.

Table 3. *Stability Constants for Complexes of* **I**, **II**, **1a**–**c**, *Benzo[12]crown-4* (B[12]C4), *Benzo[15]crown-5* (B[15]C5), *and Benzo[18]crown-6* (B[18]C6) *with Metal Cations*[a])

	Cation	$C_L \cdot 10^6$/M	C_M/M	β[b])/M	logK_1 (logK_2)	Ref.
I	Mg^{2+}	4	0–0.001	0.01	5.23	[6]
	Ca^{2+}	4	0–0.001	0.01	4.78	[6]
	Sr^{2+}	4	0–0.001	0.01	4.43	[6]
	Ba^{2+}	4	0–0.001	0.01	4.39	[6]
II	Li^+	7	0–0.1		1.96	[11]
	Na^+	7	0–0.1		1.40	[11]
	Ca^{2+}	7	0–0.1		2.28	[11]
1a	Li^+	20	0–0.1	0.1	1.50	
	Na^+	20	0–0.1	0.1	1.80	
1b	Li^+	15	0–0.01	0.1	4.16	
	Na^+	15	0–0.01	0.1	3.89	
	K^+	15	0–0.001	0.1	3.11	
	Mg^{2+}	3	0–0.001	0.01	5.95	
	Ca^{2+}	3–15	0–0.001	0.01	5.14	
	Sr^{2+}	3–80	0–0.001	0.01	4.92 (4.91)	
	Ba^{2+}	3–70	0–0.001	0.01	4.69 (4.42)	
1c	Li^+	15	0–0.1	0.1	1.98	
	Na^+	15	0–0.001	0.1	4.68	
	K^+	15	0–0.001	0.1	4.81	
B[12]C4	Li^+				1.05	[21][22]
	Na^+				1.88	[21][22]
	K^+				1.76	[21][22]
B[15]C5	Li^+				4.46	[23]
	Na^+				4.25	[23]
	K^+				2.49	[23]
	Mg^{2+}	10		$<10^{-4}$	7.2 ± 0.3	[24]
	Ca^{2+}	10		$<10^{-4}$	6.6 ± 0.2	[24]
B[18]C6	Li^+				1.8	[21]
	Na^+				4.71	[21]
	K^+				4.75	[21]

[a]) In MeCN at 25°. [b]) β = Ionic strength.

The behavior of CBD **1b** toward complexation with alkaline earth metal cations resembles, at the qualitative level, that of CSD **I**. In both cases, complex formation results in a hypsochromic shift of the long-wavelength absorption band and the luminescence spectrum, and also in a decrease in the luminescence quantum yield. The optical response and stability of 1:1 complexes for both dyes increase as the metal-cation diameter decreases. The difference between the structures of dyes **I** and **1b** manifests itself in the analysis of quantitative data. The magnitudes of the spectral shifts for complexes **1b** in energy units (cm^{-1}) are smaller, while the stability of the 1:1 complexes is much higher. The main reason for the increase in the stability of metal complexes of **1b** is probably the decrease in the electron-withdrawing effect of the positively charged benzothiazolium residue on the benzocrown fragment caused by lengthening of the conjugation chain. *Table 3* also contains published data on the stability constants of complexes of unsubstituted benzo[12]crown-4 (B[12]C4), benzo[15]crown-5 (B[15]C5), and benzo[18]crown-6 (B[18]C6). Analysis of these

data shows that the introduction of the positively charged dye fragment into the benzocrown ether has only a slight influence on the stability of complexes with alkali-metal cations. However, the stability of complexes with alkaline earth metal cations decreases by more than an order of magnitude on passing from B[15]C5 to dye **1b**. The selectivity of complex formation barely changes upon introduction of a dye fragment into the benzocrown ether.

Modeling. To estimate the influence of complexation on the dye structure and on the conformational equilibrium between *anti*- and *syn*-isomers, DFT calculations for 1:1 complexes of **1b** with the Mg^{2+} ion with full optimization of the geometry were carried out (*Tables 1* and *4*). This complex was chosen for the calculation due to the fact that it has the highest thermodynamic stability among the other metal complexes of **1b** (*Table 3*) and shows the relatively large shift of the long-wavelength absorption maximum (*Table 2*). Each of the calculated structures had $3N-6$ ($N=67$ atoms) positive harmonic vibrational frequencies, indicating that each structure corresponds to a local minimum of the PES. The calculation showed that the complexes [Mg{*anti*-(*E*,*E*)-**1b**}]$^{2+}$ and [Mg{*syn*-(*E*,*E*)-**1b**}]$^{2+}$, like the initial dye molecules, are thermodynamically the most favorable isomers; the butadiene fragment is nearly planar, as in the free dye molecules. The coordination polyhedron of the Mg^{2+} in the crown-ether moiety of the dye resembles a distorted tetragonal pyramid, the electron densities of all the five Mg···O bonds being approximately equivalent.

Table 4. *DFT-Calculated Selected C–C Bond Lengths* [Å] *in* syn- *and* anti-*Conformers of* (E,E)-**1b** *and Their* Mg^{2+} *Complexes*

	anti-(*E*,*E*)-**1b**	*syn*-(*E*,*E*)-**1b**	[Mg{*anti*-(*E*,*E*)-**1b**}]$^{2+}$	[Mg{*syn*-(*E*,*E*)-**1b**}]$^{2+}$
C(2)–C(a)	1.409	1.409	1.433	1.434
C(a)–C(b)	1.386	1.386	1.369	1.368
C(b)–C(c)	1.407	1.407	1.432	1.433
C(c)–C(d)	1.382	1.382	1.365	1.365
C(d)–C(1′)	1.430	1.429	1.459	1.457

Comparison of the total-energy differences of the pairs of free dyes with those of the complexes showed that the inclusion of Mg^{2+} in the coordination sphere of the crown-ether fragment results in a greater energy difference between the *anti*- and *syn*-isomers of **1b**. Thus, the complex of the *anti*-form of the dye becomes energetically more favorable by 2 kcal/mol than the complex formed by the *syn*-isomer. Calculation by the *Boltzmann* formula indicates that complex formation increases the contribution of the *anti*-isomer to the conformation equilibrium from 35.8% for free dye to 96.5% for the [Mg{(*E*,*E*)-**1b**}]$^{2+}$ complex (see *Scheme 4*).

An increase in the difference between the energies of *anti*- and *syn*-**1b** following the complex formation is due to the decrease in the degree of π-electron density delocalization in the butadiene fragment of the dye upon complexation. This manifests itself as shortening of the C=C bonds and elongation of the single bonds on going from the metal-free dye to the complex (*Table 4*).

The bond orders are subject to similar changes. On passing from the free dye to its complex, the electron density on the C=C bonds increases, while that on the single bonds decreases. The main reason for the fact that the *anti*-isomer proves to be

Scheme 4

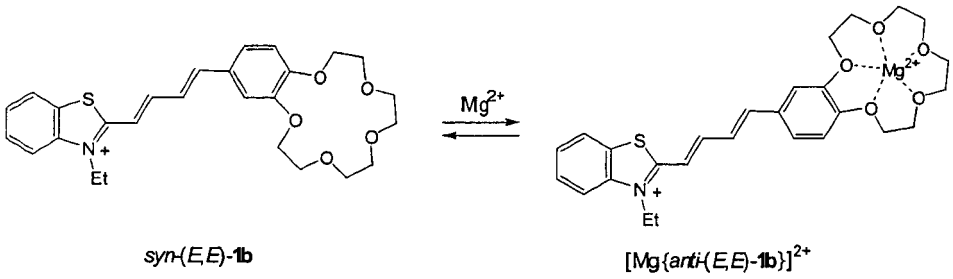

syn-(*E*,*E*)-**1b** [Mg{*anti*-(*E*,*E*)-**1b**}]$^{2+}$

thermodynamically more stable in the case of complexes is that, in this isomer, the distance between the two positively charged fragments of the molecule is 0.8 Å longer than that in the *syn*-isomer and, consequently, the coulombic repulsion between them is weaker.

It is evident that, if complexation brings about a decrease in the degree of delocalization of the π-electron density in the butadiene fragment, the hypsochromic shift of the absorption band in the electronic spectrum should be favored. According to ZINDO/S calculations of the energy of the first singlet transition for *anti*-(*E*,*E*)-**1b** ($\Delta E_{S_0 \rightarrow S_1}$, 483 nm) and its complex with Mg^{2+} ($\Delta E_{S_0 \rightarrow S_1}$, 464 nm), the hypsochromic shift of the band in the electronic spectrum induced by complex formation amounts to 19 nm. Although the actual hypsochromic shift, $\Delta\lambda = 38$ nm (*Table 2*), is twice as great as the calculated one, the DFT calculated data on the changes of the electronic and geometry structure in the butadiene moiety of the dye following an insertion of the metal ion into the crown cavity are in agreement with reality.

Dye **1b** is more prone than CSD **I** to form sandwich-type 2 : 1 complexes (dye **I** does not form these complexes at $C_L \approx 10^{-6}$ M). It is noteworthy that the formation of 2 : 1 complexes leads to a greater shift in the absorption maximum of **1b** than the formation of 1 : 1 complexes with the same metal ion. Comparison of the absorption spectra of [Ba(**1b**)]$^{2+}$ and [Ba(**1b**)$_2$]$^{2+}$ (*Fig. 4*) suggests that this is due to splitting of the absorption band of the sandwich complex, which is caused by through-space interaction of two dye molecules in [Ba{(*E*,*E*)-**1b**}$_2$]$^{2+}$. The band with a lower transition energy has a low intensity and displays itself as a shoulder at the higher-energy band. It follows from the exciton theory that the angle between the two chromophore systems in the sandwich complex is much smaller than 90°; in other words, the dye molecules are located one above another, as in the *H*-type dimers of cyanine dyes [8]. A similar spectral pattern has been observed in our previous study dealing with intramolecular sandwich complexes of the covalently linked dimers of CSD [5][6], in which the angle between the chromophore systems is obviously smaller than 90° for steric reasons.

Raman *Study*. To evaluate the type of interaction of the chromophores in the sandwich complexes of dye **1b** and to establish their structure in more detail, additional studies were undertaken. The complexation of dye **1b** with alkali (Li^+, Na^+) and alkaline earth (Mg^{2+}, Ca^{2+}, Sr^{2+}, Ba^{2+}) metal perchlorates in MeCN solutions was studied by resonance *Raman* (RR) spectroscopy. The RR spectrum of **1b** (*Fig. 5*, *a*) exhibits a set of intense bands in the 980 – 1630 cm^{-1} range and no intense bands in the low-frequency region. The vibrational frequencies of **1b** were assigned resorting to the

results of the comprehensive analysis of the structurally similar dye **I** [25][26]. According to this analysis, the bands can be classified into those related to *all-trans*-diphenylbutadiene-like (DPB) fragment and the bands originating from the benzothiazolium fragment. The benzene modes of benzo[15]crown-5 are among the modes assigned to the DPB-like fragment; the modes of the crown ether are not enhanced, except for the Ph–O stretching mode. Replacement of the ethylene bridge with the butadiene bridge is the only structural difference between **1b** and the dye **I**. This replacement makes the central unit in **1b** even more similar to DPB and simplifies the RR spectrum. The contribution of the vibrational modes of the benzothiazolium fragment to the spectrum of **1b** diminishes, and the modes attributed solely to the DPB-like fragment become predominant (*Table 5*). Instead of the 8a and 8b doublet benzene mode (*Wilson* notation) typical of dye **I**, the single intense 8a mode is observed for **1b**; the presence of the very weak 8b mode can be revealed only after digital deconvolution of the **1b** spectrum into constituent bands.

The interaction of **1b** with any of the studied cations was manifested as a change in the $I(1270)/I(1287)$ intensity ratio of the 1270 and 1287 cm^{-1} bands and a shift of the 1574 cm^{-1} band to longer wavelengths (*Fig. 5*, *b*–*d*). The $I(1270)/I(1287)$ ratio gradually diminishes from 1.1 to *ca.* 0.6 upon the addition of metal cations to **1b**. Simultaneously, the 1574 cm^{-1} band shifts to 1588 cm^{-1} for the Mg^{2+} ion (*Fig. 5*, *d*) and to 1582 cm^{-1} for Ba^{2+}, Sr^{2+}, Ca^{2+}, Na^{+}, and Li^{+} (*Fig. 5*, *c*). Deconvolution of the 1500–1630 cm^{-1} region of the spectra into constituent bands demonstrated that the apparent shift of the 1574 cm^{-1} band is actually a decrease in the intensity of this band accompanied by an increase in the intensity of the 1582 cm^{-1} band (or 1588 cm^{-1}, for Mg^{2+}). The contribution of the 1574 cm^{-1} band vanishes for high C_M/C_L ratios; thus, this

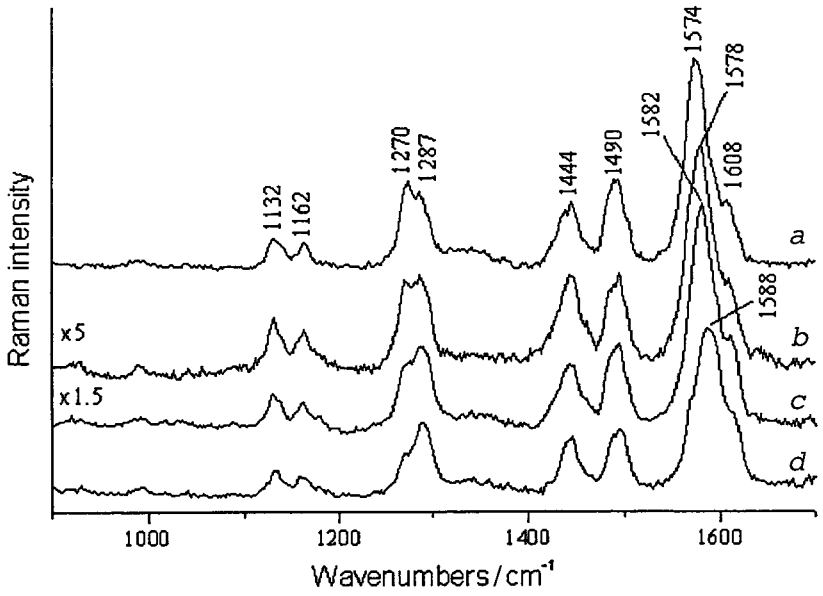

Fig. 5. *Resonance Raman spectra of* a) **1b** *and its complexes with* b) c) Ba^{2+} *and* d) Mg^{2+} *in MeCN*; $C_L = 2 \cdot 10^{-4}$ M, $C_M/C_L = 2.5$ (*b*)) and 25 (*c*), *d*)). The contribution of MeCN is subtracted.

Table 5. *Frequencies and RR Cross-Sections of the Vibrational Modes of* **1b** *and Its Complexes*[a]) *with Metal Cations*

1b	[Li(**1b**)]$^+$	[Na(**1b**)]$^+$	[Mg(**1b**)]$^{2+}$	[Ca(**1b**)]$^{2+}$	[Sr(**1b**)]$^{2+}$	[Sr(**1b**)$_2$]$^{2+}$	[Ba(**1b**)]$^{2+}$	[Ba(**1b**)$_2$]$^{2+}$	Assignment[e])	DPB[f])
1131[b]) (202)[c])	*−1* (133)	*−1*[d]) (164)	*+1* (121)	*0*[d]) (193)	*0* (135)	*0* (91)	*+1* (135)	*+1* (82)	C−C str.[h]) in phase	1141, 1134
1162 (186)	*−2* (130)	*−1* (140)	*−2* (86)	*+1* (114)	*+1* (89)	*+1* (60)	*+1* (95)	*+2* (56)	15[i]), C−C−H def.	1160, 1172
1270 (497)	*−4* (234)	*−3* (159)	*−8* (94)	*−2* (187)	*−2* (142)	*−2* (109)	*0* (189)	*−1* (127)	Ph−O	1259[g])
1287 (447)	*+1* (412)	*0* (472)	*+2* (342)	*+1* (506)	*+2* (324)	*0* (154)	*+3* (334)	*+2* (123)	C−C str., out of phase	1287, 1280
1440 (440)	*−1* (435)	*−1* (380)	*0* (261)	*+1* (355)	*+2* (244)	*−1* (126)	*+3* (271)	*0* (112)	19b, ring str. and def.	1452, 1444
1490 (657)	*−1* (386)	*−1* (449)	*+3* (253)	*+1* (397)	*+2* (307)	*0* (155)	*+3* (351)	*0* (112)	19a, ring str.	1495, 1492
1574 (1539)	*+7* (1216)	*+6* (1265)	*+14* (897)	*+7* (1138)	*+7* (892)	*+3* (401)	*+7* (970)	*+7* (278)	8a, ring str.	1577, 1585
1592[j]) (190)									8b, ring str.	1595,
1607 (384)	*+5* (267)	*+5* (240)	*+7* (305)	*+6* (274)	*+5* (165)	*+4* (90)	*+7* (230)	*+7* (72)	C=C str.	1625, 1615

[a]) Parameters of the complexes were calculated after subtraction of free dye contribution (if any). [b]) Frequencies of vibrational modes, in cm^{-1}. [c]) The values in parentheses are the RR cross-sections of the modes excited at 457.9 nm, in mbarn sr^{-1} molecule^{-1}. [d]) The shifts of the bands on complexation with metal cations are indicated in *italics*, in cm^{-1}. [e]) Assignments based on data from [25][26]. [f]) Frequencies of all-*trans*-diphenylbutadiene in solution/solid state, in cm^{-1} [25][27]. [g]) [25]. [h]) str. = stretching mode, def. = deformation mode. [i]) The benzene modes are numbered in terms of the *Wilson* notation. *j*) The parameters of the 8b mode were not defined for complexes because of the substantial overlap with the neighboring intense bands.

band can be used as a marker for the presence of metal-free dye in M^{m+}/**1b** mixtures. Accordingly, when calculating the real spectra of metal complexes of **1b**, the contribution of the metal-free dye was subtracted whenever necessary after normalization to the 1574 cm^{-1} band (*Table 5*).

The spectra of the 1:1 complexes were calculated from the experimental spectra recorded at high C_M/C_L ratios ranging from 10 to 25, *i.e.* under conditions where the 1:1 complexes predominate according to UV/VIS data. The contribution of the free-ligand signal to these experimental spectra was perceptible in the case of Na^+ and Li^+ and negligible for alkaline earth metal cations. This attests qualitatively to higher stability constants for complexes of **1b** with alkaline earth metal cations compared to those for complexes with alkali metal cations (*Table 3*). It should be mentioned that 1:1 complexations with Mg^{2+}, Ba^{2+}, and Sr^{2+} lead to more pronounced decrease in the RR cross-sections of ligand modes than binding with Na^+ or Li^+ (*Table 5*). This can be related to stronger charge-dipole interactions between the doubly charged cations and the π-electronic system of the chromophore.

Whereas the patterns of changes in the relative intensity and the positions of bands were fairly similar for complexes with various cations, the dependencies of the RR signal intensity on the C_M/C_L ratio were essentially different for particular types of cations (*Fig. 6*). The intensity of the RR signal was little affected by the addition of Na^+ and Li^+ cations to **1b**. A smooth gradual decrease in the signal intensity was observed upon an increase in the C_M/C_L ratio for Mg^{2+} and Ca^{2+}. An unusual dependence was found for Sr^{2+} and Ba^{2+}. Thus, the RR signal intensity dropped at low C_M/C_L ratios and built up upon the increase in the C_M/C_L ratio. Finally, at high C_M/C_L ratios, the RR signal intensities coincided for all the alkaline earth metal cations studied.

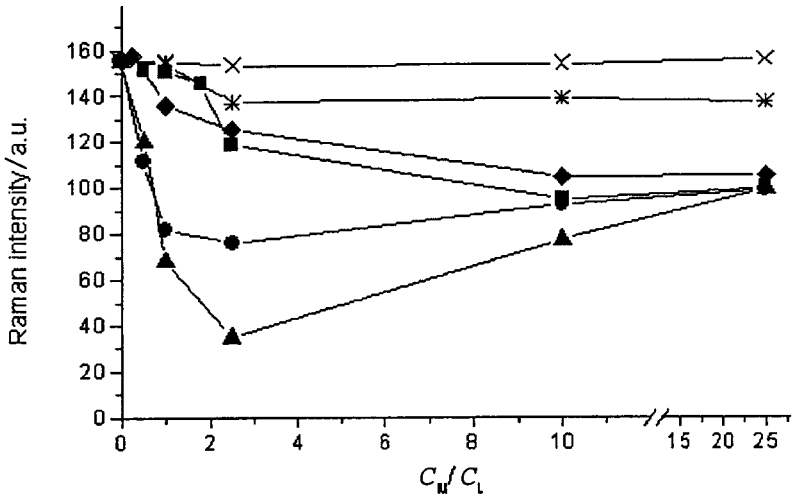

Fig. 6. *Integrated intensity of the RR signal of* **1b** *as a function of the* C_M/C_L *ratio for* Li^+ (*), Na^+ (×), Mg^{2+} (◆), Ca^{2+} (■), Sr^{2+} (●), *and* Ba^{2+} (▲); $C_L = 2 \cdot 10^{-4}$ M, λ_{exc} 457.9 nm

It was concluded that the complex formation between **1b** and Ba^{2+} (Sr^{2+}) involves an important feature not inherent in the complexation of **1b** with Ca^{2+} (Mg^{2+}). This feature is observable at low C_M/C_L ratios and disappears upon an increase in the metal cation concentration. The simulated spectrum of the $[Ba(\mathbf{1b})]^{2+}$ ($[Sr(\mathbf{1b})]^{2+}$) complex formed at low C_M/C_L ratio was found to be very similar to the spectrum measured at high C_M/C_L ratio, except for the RR cross-sections of vibrational modes (*Table 5*). Therefore, the existence of two types of complexes has to be assumed. The complex between **1b** and Ba^{2+} (Sr^{2+}) formed at low C_M/C_L ratio is characterized by *ca.* three times (or two times) lower RR cross-sections than that existing at high C_M/C_L ratio. This dual behavior can be explained by the fact that the large Ba^{2+} (Sr^{2+}) ions, unlike the small Mg^{2+} (Ca^{2+}) ions, are able to interact with two **1b** molecules to form sandwich-type 2:1 complexes. In the case of Ba^{2+} (Sr^{2+}), an increase in the C_M/C_L ratio provokes dissociation of the 2:1 complex and stabilizes the ordinary 1:1 complex. The considerable decrease in the RR cross-sections upon formation of the 2:1 complex attests to a noticeable inter-chromophore interaction, which could occur only if the π-electronic systems of molecules **1b** bound in the complex overlap, at least, partially.

NMR Study. ^{1}H-NMR Spectroscopy provides more comprehensive information on the structure of metal complexes of the crown compounds [28]. *Table 6* presents ^{1}H-NMR data for the complexes $[Mg\{(E,E)\text{-}\mathbf{1b}\}]^{2+}$, $[Sr\{(E,E)\text{-}\mathbf{1b}\}]^{2+}$, and $[Sr\{(E,E)\text{-}\mathbf{1b}\}_2]^{2+}$ in CD_3CN. The addition of excess magnesium perchlorate to a solution of (*E*,*E*)-**1b** in CD_3CN results in downfield shifts of most of the signals in the ^{1}H-NMR spectrum (*Table 6*). The greatest shift (by 0.32 – 0.43 ppm) is found for the protons of methylene groups, especially those located in the α- and α'-positions of the crown-ether fragment to which the metal cation is directly attached.

As the distance to the Mg^{2+} ion residing in the macrocycle cavity increases, the electron-withdrawing influence of this ion is attenuated, and the changes in the chemical shift decrease. The downfield shifts of the benzene-ring protons amount to

Table 6. *^{1}H-NMR Spectroscopy Data for Dye (*E,E*)-***1b*** and Its Complexes with $Mg(ClO_4)_2$ and $Sr(ClO_4)_2$*[a])

	δ/ppm										
	H–C(4)	H–C(5)	H–C(6)	H–C(7)	H–C(a)	H–C(b)	H–C(c)	H–C(d)	H–C(2′)	H–C(5′)	H–C(6′)
(*E*,*E*)-**1b**	8.04	7.87	7.77	8.19	7.21	7.92	7.26	7.36	7.27	7.03	7.27
[Mg{(*E*,*E*)-**1b**}]$^{2+}$	8.06	7.86	7.76	8.20	7.40	7.91	7.47	7.37	7.54	7.26	7.43
$\Delta\delta_{Mg}$[b])	0.02	−0.01	−0.01	0.01	0.19	−0.01	0.21	0.01	0.27	0.23	0.16
[Sr{(*E*,*E*)-**1b**}]$^{2+}$	8.06	7.86	7.77	8.20	7.36	7.91	7.43	7.38	7.53	7.25	7.43
$\Delta\delta_{Sr}$[b])	0.02	−0.01	0.00	0.01	0.15	−0.01	0.17	0.02	0.26	0.22	0.16
[Sr{(*E*,*E*)-**1b**}$_2$]$^{2+}$	7.94	7.78	7.64	7.96	7.32	7.86	7.27	7.27	7.06	7.06	7.33
$\Delta\delta_{Sr}$[b])	−0.10	−0.09	−0.13	−0.23	0.11	−0.06	0.01	−0.09	−0.21	0.03	0.06

	δ/ppm						
	CH_2N	Me	H–C(α)	H–C(α′)	H–C(β)	H–C(γ)	H–C(δ)
(*E*,*E*)-**1b**	4.71	1.59	4.21	4.21	3.88	3.72	3.69
[Mg{(*E*,*E*)-**1b**}]$^{2+}$	4.74	1.57	4.64	4.57	4.21	4.06	4.01
$\Delta\delta_{Mg}$[b])	0.03	−0.02	0.43	0.36	0.33	0.34	0.32
[Sr{(*E*,*E*)-**1b**}]$^{2+}$	4.75	1.58	4.53	4.48	4.05	3.98	3.95
$\Delta\delta_{Sr}$[b])	0.04	−0.01	0.32	0.27	0.17	0.26	0.26
[Sr{(*E*,*E*)-**1b**}$_2$]$^{2+}$	4.71	1.56	4.43	4.28	4.02	4.02	4.01
$\Delta\delta_{Sr}$[b])	0.00	−0.03	0.22	0.07	0.14	0.30	0.32

[a]) In CD_3CN at 60°, complex [Mg{(*E*,*E*)-**1b**}]$^{2+}$ was obtained at $C_L = 5 \cdot 10^{-3}$ M and $C_M = 5.5 \cdot 10^{-3}$ M; [Sr{(*E*,*E*)-**1b**}]$^{2+}$ was obtained at $C_L = 5 \cdot 10^{-3}$ M and $C_M = 0.2$M; [Sr{(*E*,*E*)-**1b**}$_2$]$^{2+}$ was obtained at $C_L = 0.02$M and $C_M = 0.01$M. [b]) $\Delta\delta_M = \delta$ (complex) $- \delta$ (ligand).

0.16–0.27 ppm, while those for the H–C(a) and H–C(c) protons of the butadiene moiety are 0.19–0.21 ppm. The substantial shift of the signals of the H–C(a) and H–C(c) protons is evidently related to the decrease in the electron density on even C-atoms in the conjugated polymethine chain, which experience the greatest mesomeric effect from the O-atom located in the *para*-position. The protons attached to odd C-atoms of the butadiene fragment, H–C(b), H–C(d), and the protons of the benzothiazole residue are relatively insensitive to complex formation. The pattern of variation of the ^{1}H-NMR chemical shifts caused by the formation of the [Sr{(*E*,*E*)-**1b**}]$^{2+}$ complex is the same as for the [Mg{(*E*,*E*)-**1b**}]$^{2+}$ complex (*Table 6*). The somewhat smaller magnitude of these changes is associated apparently with the lower charge density on the larger Sr^{2+} cation compared to the Mg^{2+} cation.

A different situation was observed in the formation of the [Sr{(*E*,*E*)-**1b**}$_2$]$^{2+}$ complex. The ^{1}H-NMR spectrum of this complex at room temperature was a set of appreciably broadened signals. This may be indicative of the presence of complexes containing dye molecules in different conformation states, the exchange processes between them being relatively slow on the ^{1}H-NMR time scale (500 MHz). As the temperature was raised, the spectral lines were markedly narrowed down and their number reduced to one set, which allowed the assignment of each proton of **1b** (*Table 6*). Attention is drawn by the abnormal behavior of the signals for the benzothiazole protons, the H–C(b) and H–C(d) protons of the butadiene fragment, and the H–C(2′) proton of the benzene fragment. Unlike the proton signals of the 1:1 complex, these signals shift upfield.

The results obtained suggest that the planar chromophore fragments of two molecules **1b** in the [Sr{(*E*,*E*)-**1b**}$_2$]$^{2+}$ complex are located in space mainly above one another as a result of weak intermolecular π-π interactions (stacking interactions) [29].

With this mutual arrangement, some of the unsaturated and aromatic protons of one molecule **1b** fall in the area of shielding of the conjugated unsaturated fragment of the other molecule, which is responsible for the upfield shifts of the proton signals observed. It follows from the data of *Table 6* that all the protons of the benzothiazole residue get in the area of shielding. Taking into account the fact that the crown-ether fragments in the sandwich complexes should be arranged in space above one another [5], four symmetrical structures of the sandwich complex formed by the pairs of *syn*-(*E*,*E*)- or *anti*-(*E*,*E*)-**1b** conformers can be conceived. Only one of them, [Sr{*anti*-(*E*,*E*)-**1b**}$_2$]$^{2+}$ (*Scheme 5*), complies with all the observed changes in the ^{1}H-NMR chemical shifts; thus, this structure is the most stable in MeCN solutions.

Scheme 5

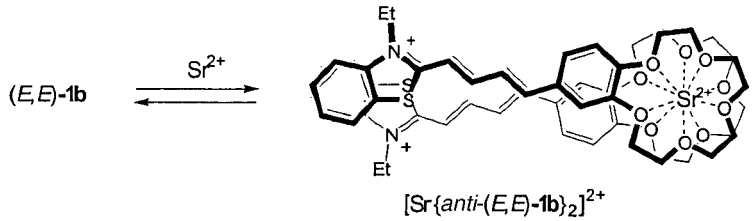

The structure of the [Sr{*anti*-(*E*,*E*)-**1b**}$_2$]$^{2+}$ complex appears unusual because two positively charged heterocyclic benzothiazolium residues are located one above another despite the electrostatic repulsion. This becomes possible, apparently, owing to the fact that the perchlorate counter ions form either solvent-separated, or more likely, contact ion pairs with the positively charged centers of the sandwich complex and thus counterbalance them. An additional contribution to the compensation of positive charges due to the ion-dipole interactions can be made by MeCN, which is a highly polar aprotic solvent. With the electrostatic repulsion being levelled out and with the short distance between the dye molecules in the sandwich complex, stabilization of the eclipsed conformation due to the direct through-space intermolecular overlap of *p*-orbitals (*i.e.*, due to the secondary orbital interactions) comes to the fore.

3. Conclusions. – The synthesis of a series of butadienyl dyes containing a benzocrown-ether fragment was developed. These compounds belong to a promising but poorly studied new type of chromoionophores. A detailed structure – property analysis for the dyes **1a** – **d** and their complexes was performed. The crown-containing butadienyl dyes synthesized exhibited a high affinity and selectivity toward alkali and alkaline earth metal cations; this allows one to expect that dyes of this structure could be used as effective chromo- and fluoroionophores. In the case of the dye containing a [15]crown-5-ether fragment, self-assembly of stable sandwich complexes according to an unusual 'head-to-head' pattern takes place with participation of two types of interaction, namely, complexation with the metal ion and stacking interactions of the planar dye fragments. The elucidated regular features of the self-assembly of complex supramolecular structures based on crown-containing butadienyl dyes demonstrate the prospects for using these compounds as structural elements in the design of photo-switchable molecular devices.

We are grateful to the *U.S. Civilian Research and Development Foundation* (Project No. RC0-872), the *Royal Society*, the *Russian Foundation for Basic Research* (Projects No. 00-03-32898, 01-03-06159, and 01-03-32474), and the *Ministry for Science and Technologies of Russia* for financial support and to the *EPSRC* for a Senior Research Fellowship (*J. A. K. H.*).

Experimental Part

1. *General*. Crown-ether cinnamaldehydes **3a**–**c** were prepared from the corresponding crown-ether benzaldehydes according to the protocol reported in [14]. The 3-ethyl-2-methyl-1,3-benzothiazol-3-ium perchlorate (**2**) was obtained by reprecipitation of 3-ethyl-2-methyl-1,3-benzothiazol-3-ium iodide [11] by perchloric acid (70%) from a MeOH/Et_2O mixture. The Mg, Ca, Sr, and Ba perchlorates (*Aldrich*) were dried *in vacuo* at 230°. Et_4NClO_4 was prepared from $HClO_4$ and Et_4NOH and twice recrystallized from H_2O and dried *in vacuo* at 50°. MeCN (for spectrophotometry, transmission $\lambda \geq 195$ nm) was dehydrated by distillation from CaH_2. The yields are given relative to salt **2**. M.p.: in a capillary; *Meltemp-II* apparatus; uncorrected. UV/VIS: *Specord M40* spectrophotometer coupled with a PC; solns. of **1a**–**d** in anh. MeCN, prepared and used in a dark room under red light. Luminescence: *Elumin* spectrofluorometer coupled with a PC; the spectra were corrected by means of the known radiation spectrum of a calibrated filament lamp with a sapphire window; dye **I** was used as the reference to determine the quantum yields [2] (error *ca.* 20%). ^{1}H-NMR: *Bruker DRX-500* spectrometer; in (D_6)DMSO, CD_3CN, and $CDCl_3$; the δ values in ppm are referred to the solvent as the internal reference (2.50 ppm for (D_6)DMSO, 1.96 ppm for CD_3CN, and 7.27 ppm for $CDCl_3$); the J values are expressed in Hz. ^{1}H,^{1}H-COSY and NOESY Experiments: pulse sequences given by *Bruker*. Elemental analyses were performed at the microanalytical laboratory of the A. N. Nesmeyanov Institute of Organoelement Compounds in Moscow, Russia.

2. *Complex Formation*. The stoichiometry of complex formation of dyes **1a**–**c** with metal ions and the stability constants of complexes were determined from the data of spectrophotometry by the matrix algebra methods: The input data for the calculations were represented by a matrix whose columns were the absorption spectra recorded for solutions with a constant total dye concentration (C_L) and a variable total concentration of a metal perchlorate (C_M). The spectra were measured over the 30000–18000 cm^{-1} range in 80-cm^{-1} increments at a constant temperature (25°) in 5-, 1-, and 0.2-cm quartz cells. The ionic strength of the solns. was maintained at 0.01M for alkaline earth metal ions and at 0.1M for alkali metal ions with Et_4NClO_4 as the supporting electrolyte [18].

3. *Resonance* Raman *Spectroscopy*. The spectra were recorded with a single-channel *Ramanor HG-2S* spectrometer with an Ar^+ laser (*Spectra-Physics*, model *164-03*; laser power 20 mW, excitation wavelength 457.9 nm). Panoramic spectra were recorded in the 200–1700 cm^{-1} range at 1-cm^{-1} increments with an integration time of 1 s. The 900–1700 cm^{-1} spectral region was recorded during titration. The MeCN band at 918 cm^{-1} was used as an internal standard of *Raman* intensity, and the RR cross-sections for the vibrational modes of **1b** were calculated from *Eqn. 3*, where the subscript n (s) implies that the parameter corresponds to the vibrational mode of **1b** (the 918 cm^{-1} band of the internal standard), σ_n is the *Raman* cross-section for the vibration mode n at an excitation wavelength of 457.9 nm, I is the peak intensity of the *Raman* band, and C_s and C_n are the molar concentrations of MeCN (19.15M) and **1b** ($2 \cdot 10^{-4}$ M), resp. In the calculation of the *Raman* cross-sections for M^{m+}/**1b** complexes, the contribution of free ligand was subtracted from the spectra of complexes whenever necessary, and the concentration of the bound ligand was taken as C_n. The *Raman* cross-section (σ_s) of the MeCN vibrational mode at 918 cm^{-1} for 457.9 nm was calculated with the parameters reported in [30]; this gave $1.99 \cdot 10^{-30}$ cm^{-2} sr^{-1} $molecule^{-1}$.

$$\sigma_n(457.9) = (I_n\ \sigma_s\ C_s)/(I_s\ C_n) \tag{3}$$

4. *Syntheses. 3-Ethyl-2-[(1*E*,3*E*)-4-(2,3,5,6,8,9-hexahydro-1,4,7,10-benzotetraoxacyclododecin-12-yl)buta-1,3-dienyl]-1,3-benzothiazol-3-ium Perchlorate* (**1a**). A mixture of salt **2** (67 mg, 0.24 mmol), cinnamaldehyde **3a** (80 mg, 0.29 mmol), and anh. EtOH (10 ml) was refluxed for 50 h. After cooling down to 5°, the precipitate formed was filtered, washed with cold EtOH and benzene, and recrystallized from anh. EtOH to give **1a** (39 mg, 30%). Reddish brown crystals. M.p. 192–194°. ^{1}H-NMR (500.13 MHz, (D_6)DMSO, 25°[1]): 1.46 (t, J = 7.1, Me); 3.63 (s, 2 CH_2O); 3.73 (m, 2 CH_2CH_2OAr); 4.18 (m, 2 CH_2OAr); 4.79 (q, J = 7.1, $MeCH_2$); 7.14 (d, J = 8.3, H–C(5′)); 7.29 (d, J = 8.3, H–C(6′)); 7.35 (dd, J = 15.6, 10.4, H–C(c)); 7.41 (s, H–C(2′)); 7.43 (d, J = 15.6, H–C(d)); 7.51 (d, J = 14.8, H–C(a)); 7.77 (m, H–C(6)); 7.85 (m, H–C(5)); 8.04 (dd, J = 14.8, 10.4, H–C(b));

8.27 ($d, J = 8.4$, H–C(4)); 8.40 ($d, J = 8.1$, H–C(7)). Anal. calc. for $C_{25}H_{28}ClNO_8S$: C 55.81, H 5.25, N 2.60; found: C 55.76, H 5.22, N 2.55.

*3-Ethyl-2-[(1*E*,3*E*)-4-(2,3,5,6,8,9,11,12-octahydro-1,4,7,10,13-benzopentaoxacyclopentadecin-15-yl)buta-1,3-dienyl]-1,3-benzothiazol-3-ium Perchlorate* (**1b**) was obtained similarly to **1a** from **2** and **3b**. Yield 37%. M.p. 183–185° (EtOH). ^{1}H-NMR (500.13 MHz, (D_6)DMSO, 25°)[1]: 1.46 ($t, J = 7.2$, Me); 3.63 (s, 4 CH_2O); 3.80 (m, 2 CH_2CH_2OAr); 4.13 (m, 2 CH_2OAr); 4.79 ($q, J = 7.2$, $MeCH_2$); 7.05 ($d, J = 8.3$, H–C(5′)); 7.22 ($d, J = 8.3$, H–C(6′)); 7.30 (s, H–C(2′)); 7.35 ($dd, J = 15.3, 10.5$, H–C(c)); 7.44 ($d, J = 15.3$, H–C(d)); 7.49 ($d, J = 14.8$, H–C(a)); 7.76 (m, H–C(6)); 7.85 (m, H–C(5)); 8.04 ($dd, J = 14.8, 10.5$, H–C(b)); 8.26 ($d, J = 8.4$, H–C(4)); 8.39 ($d, J = 8.0$, H–C(7)). Anal. calc. for $C_{27}H_{32}ClNO_9S$: C 55.71, H 5.54, N 2.41; found: C 55.87, H 5.66, N 2.39.

*2-[(1*E*,3*E*)-4-(2,3,5,6,8,9,11,12,14,15-Decahydro-1,4,7,10,13,16-benzohexaoxacyclooctadecin-18-yl)buta-1,3-dienyl]-3-ethyl-1,3-benzothiazol-3-ium Perchlorate* (**1c**) was obtained similarly to **1a** from **2** and **3c**. Yield 39%. M.p. 165–167° (EtOH). ^{1}H-NMR (500.13 MHz, (D_6)DMSO, 25°)[1]: 1.46 ($t, J = 7.2$, Me); 3.53 (s, 2 CH_2O); 3.56 (m, 2 CH_2O); 3.62 (m, 2 CH_2O); 3.63 (s, 2 CH_2O); 3.79 (m, 2 CH_2CH_2OAr); 4.17 (m, 2 CH_2OAr); 4.79 ($q, J = 7.2$, $MeCH_2$); 7.06 ($d, J = 8.4$, H–C(5′)); 7.22 ($d, J = 8.4$, H–C(6′)); 7.30 (s, H–C(2′)); 7.36 ($dd, J = 15.4, 10.4$, H–C(c)); 7.44 ($d, J = 15.4$, H–C(d)); 7.49 ($d, J = 14.8$, H–C(a)); 7.76 (m, H–C(6)); 7.85 (m, H–C(5)); 8.04 ($dd, J = 14.8, 10.4$, H–C(b)); 8.26 ($d, J = 8.5$, H–C(4)); 8.40 ($d, J = 8.1$, H–C(7)). Anal. calc. for $C_{29}H_{36}ClNO_{10}S$: C 55.63, H 5.80, N 2.24; found: C 55.33, H 5.79, N 2.22.

*2-[(1*E*,3*E*)-4-(3,4-Dimethoxyphenyl)buta-1,3-dienyl]-3-ethyl-1,3-benzothiazol-3-ium Perchlorate* (**1d**) was obtained similarly to **1a** from **2** and **3d**. Yield 50%. M.p. 234–237° (EtOH). ^{1}H-NMR (500.13 MHz, (D_6)DMSO, 25°)[1]: 1.46 ($t, J = 7.2$, $MeCH_2$); 3.83 (s, 1 MeO); 3.85 (s, 1 MeO); 4.79 ($q, J = 7.2$, $MeCH_2$); 7.07 ($d, J = 8.4$, H–C(5′)); 7.23 ($d, J = 8.4$, H–C(6′)); 7.29 (s, H–C(2′)); 7.37 ($dd, J = 15.4, 10.5$, H–C(c)); 7.46 ($d, J =$ 15.4, H–C(d)); 7.51 ($d, J = 14.8$, H–C(a)); 7.76 (m, H–C(6)); 7.85 (m, H–C(5)); 8.04 ($dd, J = 14.8, 10.5$,

Table 7. *Crystal Data and Structure-Refinement Parameters of* **1c**

Empirical formula	$C_{31}H_{41}ClN_2O_{11}S$
Formula weight [g mol^{-1}]	685.17
Temperature [K]	110.0(2) K
Wavelength λ [Å]	0.71073
Crystal system	monoclinic
Space group	$P2_1/c$
Unit-cell dimensions, a [Å]	23.5124(8)
b [Å]	7.9888(3)
c [Å]	18.2442(6)
β [°]	106.058(2)
Volume [Å^3]	3293.2(2)
Z	4
Density calc. [g cm^{-3}]	1.382
Absorption coefficient [mm^{-1}]	0.242
$F(000)$	1448
Crystal size [mm]	0.40 × 0.20 × 0.05
Habitus, color	Plate, red
θ-Range for data collection [°]	2.25 to 26.00
Limiting indices	$-23 < h < 29$, $-9 < k < 9$, $-22 < l < 18$
Reflections collected/unique	17563/6415 (R(int) = 0.0941)
Absorption correction	Empirical
Max. and min. transmission	0.9880 and 0.9096
Refinement method	Full-matrix least-squares on F^2
Data, restraints, parameters	6415, 0, 568
Goodness-of-fit on F^2	0.934
Final R indices ($I > 2\sigma(I)$)	$R_1 = 0.0519$, $wR_2 = 0.1007$
R indices (all data)	$R_1 = 0.1280$, $wR_2 = 0.1169$
Extinction coefficient	0.0052(5)
Largest diff. peak and hole [e Å^{-3}]	0.337 and −0.322

H–C(b)); 8.26 (d, J = 8.5, H–C(4)); 8.39 (d, J = 8.1, H–C(7)). Anal. calc. for $C_{21}H_{22}ClNO_6S$: C 55.81, H 4.91, N 3.10; found: C 55.92, H 4.85, N 3.04.

5. *Quantum-Chemical Calculations.* The density functional theory (DFT) calculations of the equilibrium geometry and the vibration frequencies in the harmonic approximation for the molecules under study were carried out with a quantum-chemical program [31]. This was done with a generalized gradient approximation from [32] and three-exponent sets of *Gaussian*-type basis functions [33] for all atoms, optimized for the DFT calculations with the electron-density expansion over an auxiliary basis. This is an approximate approach permitting one to accelerate markedly the calculation of the coulomb and exchange-correlation components. The density functional chosen contains no empirical parameters and predicts successfully many molecular properties such as the equilibrium geometry, bond energies, and vibration frequencies [34]. The PM3 [35] and ZINDO/S [36] methods were used with sets of standard parameters.

6. *X-Ray Crystal-Structure Determination of* **1c**. The single crystals of compound **1c** were grown from aq. MeCN soln. A red crystal was covered with perfluorinated oil and mounted on a *Bruker Smart CCD* diffractometer (ω scan, 0.3° frame, 15 s/frame, 110 K). The crystal data and structure-refinement parameters are given in *Table 7*. The structure was solved by direct methods and refined by the full-matrix least-squares method based on F^2 for all data with SHELX software [37][38]. The H_2O molecules in the vicinity of the crown-ether cavity and the MeCN solvent molecule in the cavities of the crystal packing were found. H-Atoms were located objectively. All non-H-atoms were refined with anisotropic displacement parameters, H-atoms were refined with isotropic displacement parameters.

Crystallographic data (excluding structure factors) for the structure reported in this paper have been deposited with the *Cambridge Crystallographic Data Centre* as supplementary publication No. CCDC-163548. Copies of the data can be obtained, free of charge, on application to the CCDC, 12 Union Road, Cambridge CB2 1EZ, UK (Fax: int. code + 44(1223)336-033; E-mail: deposit@ccdc.cam.ac.uk).

REFERENCES

[1] H. G. Löhr, F. Vögtle, *Acc. Chem. Res.* **1985**, *18*, 65; M. Takagi, in 'Cation Binding by Macrocycles', Eds. Y. Inoue and G. W. Gokel, Marcel Dekker, New York, 1990, p. 465; M. Pietraszkiewicz, in 'Comprehensive Supramolecular Chemistry', Ed. D. N. Reinhoudt, Pergamon, Oxford, 1996, Vol. 10, p. 225; A. P. de Silva, H. Q. N. Gunaratne, T. Gunnlaugsson, A. J. M. Huxley, C. P. McCoy, J. T. Rademacher, T. E. Rice, *Chem. Rev.* **1997**, *97*, 1515; B. Valeur, I. Leray, *Coord. Chem. Rev.* **2000**, *205*, 3.

[2] M. V. Alfimov, S. P. Gromov, in 'Applied Fluorescence in Chemistry, Biology, and Medicine', Eds. W. Rettig, B. Strehmel, S. Schrader, and H. Seifert, Springer-Verlag, Berlin, 1999, p. 161.

[3] S. P. Gromov, M. V. Alfimov, *Russ. Chem. Bull.* **1997**, *46*, 611 (Engl. Transl.).

[4] M. V. Alfimov, S. P. Gromov, I. K. Lednev, *Chem. Phys. Lett.* **1991**, *185*, 455; M. V. Alfimov, S. P. Gromov, Yu. V. Fedorov, O. A. Fedorova, A. I. Vedernikov, A. V. Churakov, L. G. Kuz'mina, J. A. K. Howard, S. Bossmann, A. Braun, M. Woerner, D. F. Sears, J. Saltiel, *J. Am. Chem. Soc.* **1999**, *121*, 4992.

[5] S. P. Gromov, O. A. Fedorova, E. N. Ushakov, A. V. Buevich, I. I. Baskin, Y. V. Pershina, B. Eliasson, U. G. Edlund, M. V. Alfimov, *J. Chem. Soc., Perkin Trans. 2* **1999**, 1323.

[6] E. N. Ushakov, S. P. Gromov, O. A. Fedorova, Y. V. Pershina, M. V. Alfimov, F. Barigelletti, L. Flamigni, V. Balzani, *J. Phys. Chem. A* **1999**, *103*, 11188.

[7] S. P. Gromov, E. N. Ushakov, A. I. Vedernikov, N. A. Lobova, M. V. Alfimov, Y. A. Strelenko, J. K. Whitesell, M. A. Fox, *Org. Lett.* **1999**, *1*, 1697.

[8] In 'The Theory of the Photographic Process', Ed. T. H. James, Macmillan Publ., New York, 1977, Chapt. 8.

[9] K. Kato, *IEEE J. Quantum Electron.* **1980**, *QE16*, 1017.

[10] M. V. Bondar, N. A. Derevyanko, G. G. Dyadyusha, V. M. Zibarovskii, A. A. Ishchenko, O. V. Przhonskaya, Yu. L. Slominskii, A. L. Smirnova, E. A. Tikhonov, A. I. Tolmachev, *Kvantovaya Elektronika* **1984**, *11*, 462 (*Sov. J. Quantum Electronics* **1984**, *11*, 317 (Engl. Transl.)).

[11] S. P. Gromov, S. A. Sergeev, S. I. Druzhinin, M. V. Rusalov, B. M. Uzhinov, L. G. Kuz'mina, A. V. Churakov, J. A. K. Howard, M. V. Alfimov, *Russ. Chem. Bull.* **1999**, *48*, 525 (Engl. Transl.).

[12] S. I. Druzhinin, M. V. Rusalov, B. M. Uzhinov, S. P. Gromov, S. A. Sergeev, M. V. Alfimov, *J. Fluor.* **1999**, *9*, 33.

[13] E. N. Ushakov, S. P. Gromov, O. A. Fedorova, M. V. Alfimov, *Russ. Chem. Bull.* **1997**, *46*, 463 (Engl. Transl.).

[14] A. I. Vedernikov, S. P. Gromov, *Synthesis* **2001**, 889.

[15] E. N. Ushakov, S. P. Gromov, A. V. Buevich, I. I. Baskin, O. A. Fedorova, A. I. Vedernikov, M. V. Alfimov, B. Eliasson, U. Edlund, *J. Chem. Soc., Perkin Trans. 2* **1999**, 601.
[16] F. H. Allen, O. Kennard, *Chem. Design Autom. News* **1993**, *8*, 1.
[17] G. R. Desiraju, *Chem. Commun.* **1997**, 1475.
[18] E. N. Ushakov, 'Ph.D. Thesis', Institute of Chemical Physics in Chernogolovka, Russian Academy of Sciences, 1995 (in Russian).
[19] L. Zimányi, A. Kulsár, J. K. Lanyi, D. F. Sears, J. Saltiel, *Proc. Natl. Acad. Sci. U.S.A*. **1999**, *96*, 4408.
[20] M. S. Islam, R. A. Pethrick, D. Pugh, M. J. Wilson, *J. Chem. Soc., Faraday Trans.* **1998**, *94*, 39.
[21] V. P. Solov'ev, N. N. Strakhova, O. A. Raevskii, '13th International Symposium on Macrocyclic Chemistry', Abstracts of Papers, Hamburg, Sept. 4–8, 1988.
[22] N. N. Strakhova, V. P. Solov'ev, O. A. Raevskii, *Koord. Khim*. **1989**, *15*, 483 (in Russian).
[23] Y. Takeda, T. Kumazawa, *Bull. Chem. Soc. Jpn*. **1988**, *61*, 655.
[24] O. B. Stanislavsky, E. N. Ushakov, S. P. Gromov, O. A. Fedorova, M. V. Alfimov, *Russ. Chem. Bull*. **1996**, *45*, 564 (Engl. Transl.).
[25] I. K. Lednev, S. P. Gromov, E. N. Ushakov, M. V. Alfimov, J. N. Moore, R. E. Hester, *Spectrochim. Acta, Part A* **1992**, *48*, 799.
[26] A. Feofanov, A. Ianoul, V. Oleinikov, S. Gromov, O. Fedorova, M. Alfimov, I. Nabiev, *J. Phys. Chem*. **1996**, *100*, 2154.
[27] B. Schrader, 'Raman-Infrared Atlas of Organic Compounds', 2 edn., VCH-Verl.-Ges., Weinheim, 1989.
[28] L. A. Fedorov, A. N. Ermakov, 'Spektroskopiya YaMR v neorganicheskom analize', in 'NMR Spectroscopy in Inorganic Analysis', Nauka, Moscow, 1989, p. 122 (in Russian).
[29] D. B. Amabilino, M. Asakawa, P. R. Ashton, R. Ballardini, V. Balzani, M. Belohradsky, A. Credi, M. Higuchi, F. M. Raymo, T. Shimizu, J. F. Stoddart, M. Venturi, K. Yase, *New J. Chem*. **1998**, *22*, 959.
[30] J. M. Dudik, C. R. Johnson, S. A. Asher, *J. Chem. Phys.* **1985**, *82*, 1732.
[31] D. N. Laikov, *Chem. Phys. Lett*. **1997**, *281*, 151.
[32] J. P. Perdew, K. Burke, M. Ernzerhof, *Phys. Rev. Lett*. **1996**, *77*, 3865.
[33] D. N. Laikov, 'Ph.D. Thesis', Moscow State University, Moscow, 2000 (in Russian).
[34] C. Adamo, V. Barone, *J. Chem. Phys*. **1999**, *110*, 6158.
[35] J. J. P. Stewart, *J. Comput. Chem*. **1989**, *10*, 209.
[36] J. Ridley, M. C. Zerner, *Theor. Chim. Acta* **1973**, *32*, 111; **1976**, *42*, 223; *J. Am. Chem. Soc*. **1980**, *102*, 589.
[37] G. M. Sheldrick, *Acta Crystallogr., Sect. A* **1990**, *46*, 467.
[38] G. M. Sheldrick, 'SHELXL-97. Program for Refinement of Crystal Structures', University of Göttingen, Germany, 1997.

Received May 28, 2001